A Mutual-Coupling-Suppressed Dual-Band Dual-Polarized Base Station Antenna Using Multiple Folded-Dipole Antenna

Xuekang Liu, *Graduate Student Member, IEEE*, Steven Gao, *Fellow, IEEE*,
Benito Sanz-Izquierdo, *Member, IEEE*, Haiwei Zhang, Lehu Wen, *Member, IEEE*, Wei Hu, *Member, IEEE*,
Qi Luo, *Senior Member, IEEE*, Josaphat Tetuko Sri Sumantyo, *Senior Member, IEEE*,
and Xue-Xia Yang, *Senior Member, IEEE*

Abstract—An interleaved shared-aperture dual-band dual-polarized base station array antenna is proposed in this article. The lower-band (LB) element is realized by using a multiple folded-dipole antenna (MFDA) and four parasitic loops. To interpret the working principle of the MFDA, a double folded-dipole antenna (DFDA) is firstly analyzed by using the transmission line (TL) model. Then, by combining two bended DFDAs and introducing four parasitic loops, a low cross-band scattering LB element with a high out-of-band rejection level of 16 dB is obtained to cover 2.3–2.7 GHz. The higher-band (HB) element with a wide impedance bandwidth of 42.5% (3.0–4.6 GHz), a high roll-off rate (*RoR*) of 249.2 dB/GHz, and a high out-of-band rejection level of 17 dB is obtained by introducing a meander line loop (MLL), a rectangular loop (RL), and V-shaped strips (VSS) near the dipole arms. By combining the proposed low-scattering low-pass LB element and the high-*RoR* high-pass HB element, a novel interleaved shared-aperture dual-band dual-polarized array antenna with a small frequency ratio of 1.46 and a high cross-band isolation level of 25 dB is realized. Due to the low-scattering characteristic and filtering response of the LB element, the radiation patterns of the wideband HB sub-arrays are almost unaffected.

Index Terms—Base station array antenna, dual-band antenna, dual-polarized antenna, filtering antenna.

Xuekang Liu, Benito Sanz-Izquierdo, and Lehu Wen are with the School of Engineering, University of Kent, CT2 7NT Canterbury, U.K. (e-mail: xl255@kent.ac.uk).

Steven Gao is with the Department of Electronic Engineering, The Chinese University of Hong Kong, Hong Kong.

Haiwei Zhang is with Huawei Technologies Ltd., Chengdu 610212, China.

Wei Hu is with the National Laboratory of Science and Technology on Antennas and Microwaves, Xidian University, Xi'an, Shaanxi 710071, China.

Qi Luo is with the School of Physics, Engineering and Computer Science, University of Hertfordshire, AL10 9AB Hatfield, U.K.

Josaphat Tetuko Sri Sumantyo is with the Center for Environmental Remote Sensing, Chiba University, Chiba 263-8522, Japan.

Xue-Xia Yang is with the School of Communication and Information Engineering, Shanghai University, Shanghai 200444, China.

Color versions of one or more figures in this article are available at https://doi.org/10.1109/TAP.2022.3209177.

Digital Object Identifier 10.1109/TAP.2022.3209177

I. INTRODUCTION

SHARED-APERTURE dual/multiband dual-polarized array antennas have become a trend in the base station application to meet the growing need for fully integrated base stations. Although the shared-aperture design can realize a dual/multiband array antenna with compact size and low cost, it also brings new design challenges, such as the high mutual couplings between the closely placed antenna elements, and the cross-band scattering between the lower band (LB) and higher band (HB) elements.

To enhance the port isolations, many new methods are investigated [1], [2], [3], [4], [5], [6], [7], [8], [9], [10], [11], [12], [13], [14], [15], [16], [17]. By introducing decoupling branches [1], [2] and decoupling surface [2], the mutual coupling in [1] and [2] is effectively reduced. In [3], [4], and [5], baffles are used to improve the isolations between the elements. To obtain high isolations and good radiation performance, the structure, position, and height, of the baffle are optimized. Using filtering antennas [6], [7], [8], [9], [10] is also a popular method to obtain high isolations in the design of dual-multiband array antenna. By properly designing the structure of the radiator [11] or integrating a filter into the transmission line (TL) [12], antenna elements with a high out-of-band rejection level can be obtained. The LB element has nearly no radiation in the operating band of the HB element and vice versa. Thus, the port isolations in the array antenna maintain a very low level. Although the methods mentioned above can enhance the port isolations in the dual/multiband array, the cross-band scattering is not fully addressed.

To reduce the cross-band scattering, a novel method is presented in [18], [19], [20], [21], and [22]. By inserting a frequency selective surface (FSS) layer between the LB and HB elements, the cross-band scatterings in [18], [19], [20], and [21] are effectively reduced. In these designs, the HB elements are usually placed above the LB element. For the HB elements, the FSS layer can be equivalent to a ground plane. However, for the LB element, the FSS layer can be seen as EM transparent structure. Thus, not only high port isolation but also low cross-band scattering can be realized

by using this method. However, the frequency ratios in these designs are larger than 4.

Apart from inserting the FSS layer, lifting the HB elements [23] using electromagnetic (EM) transparent LB elements [24], [25], [26], [27], [28], [29], [30], [31], [32] and introducing partially reflecting surfaces [33] can also reduce the cross-band scattering. By lifting the cavity-backed HB elements to the same plane of the LB radiator [23], the blockage effect of the LB element on the radiation patterns of HB elements can be eliminated. The limitation of this method is that it is not suitable for the dual-band array antenna design with a small frequency ratio. In [24] and [25], two shared-aperture dual-band array antennas are realized by introducing branches on the radiator of the LB element. By changing the length of the branches, the wave-transparent band can be easily adjusted. However, the frequency ratios of these two dual-band array antennas are larger than 2.7. By dividing the dipole arms into short sections and introducing chokes below the gaps between the short sections, a low-scattering LB element is presented in [26]. Based on this LB element, a low cross-band scattering dual-band array with a small frequency ratio of 2.19 is achieved. Two low-scattering LB elements are presented in [27] and [28] by introducing parasitic structures near the radiators. The combination of the radiator and the parasitic structure functions as a bandpass filtering circuit. Thus, at their resonant frequencies, the HB EM wave can be transmitted through the LB element without being affected. In [30] and [31], by using the FSS element as a radiator, two low-scattering LB elements are proposed. Based on these wave-transparent LB elements, two low cross-band scattering array antennas with reduced frequency ratios (1.58 and 1.42) are realized. However, the wave-transparent band of these structures is relatively narrow.

In this article, an interleaved shared-aperture dual-band dual-polarized array antenna with a low-frequency ratio (1.46), low cross-band scattering, wide wave-transparent band, and high isolations is proposed for base station application by combining the proposed LB and HB element. By utilizing multiple folded-dipole antennas (MFDAs), an LB element with a high out-of-band rejection level and low cross-band scattering is realized. The working principle of the MFDA is firstly explained in this article based on the proposed TL model of the double folded-dipole antenna (DFDA). By introducing a meander line loop (MLL), rectangular loop (RL), and V-shaped strips (VSS), a novel filtering antenna with a high Roll-off rate (RoR) is realized to cover the HB. The working principle of the MLL is analyzed in detail in this article by utilizing an equivalent circuit. To validate the performance of the proposed designs, an interleaved shared-aperture dual-band array antenna including one LB element and four HB elements is designed. The measured and simulated results demonstrate that the proposed designs maintain a good performance in the proposed dual-band array. Besides, to suppress the mutual coupling between the HB sub-arrays, eight shorted strips are introduced next to the HB elements. After introducing the shorted strips, the mutual couplings between the HB arrays can be effectively reduced to below −22 dB. All the simulations
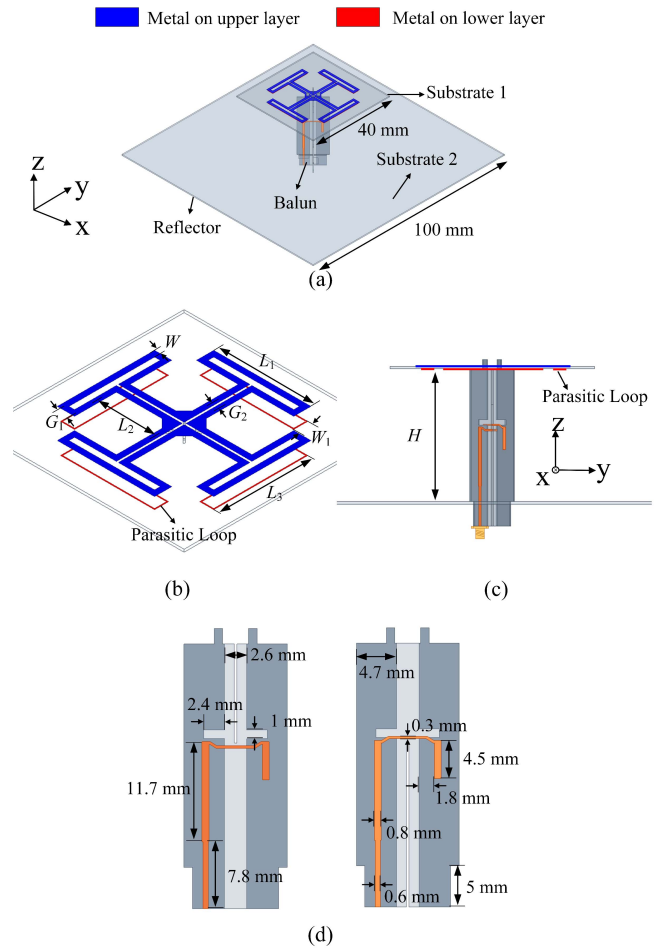

Fig. 1. Configuration of the proposed LB antenna. (a) Three-dimensional view, (b) radiator, (c) side view, and (d) balun. Dimensions are $L_1 = 18.7$, $L_2 = 11.5$, $L_3 = 18.1$, $W = 1.1$, $W_1 = 2.7$, $G_1 = 2.2$, $G_2 = 1.5$, and $H = 26$ (unit: millimeter).

in this article are completed by using the commercial EM simulation software Ansys HFSS.

II. DESIGN OF ANTENNA ELEMENTS

In this section, LB and HB antenna elements are presented for the design of the dual-band dual-polarized array antenna. The LB MFDA has a wide bandwidth, two upper radiation nulls, and innate EM transparent characteristics in HB. The HB element features wide bandwidth and a high RoR of 242.9 dB/GHz with two radiation nulls in LB.

A. LB Element

The configurations of the proposed MFDA are shown in Fig. 1. The MFDA contains two Rogers RO4003 substrates with a thickness of 0.508 mm ($\varepsilon_r = 3.55$). As can be observed, the MFDA is printed on the upper layer of substrate 1. To enhance the out-of-band rejection level, four parasitic RLs are placed under the MFDA. The configurations and dimensions of the baluns are given in Fig. 1(d). The radiator and the ground plane are connected by the feeding baluns. By using the above configuration, the proposed MFDA has
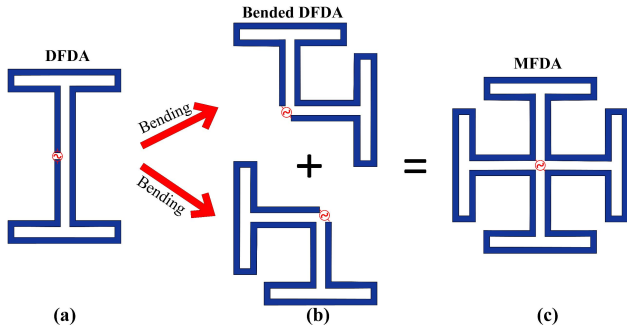
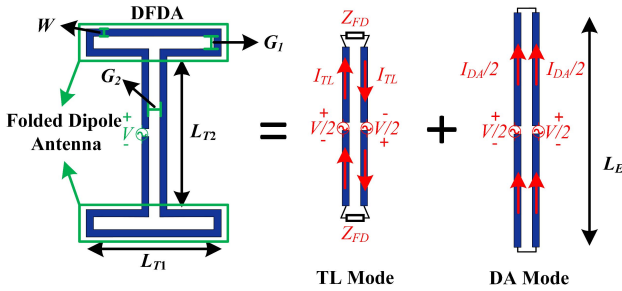Fig. 2. Evolution of the MFDA. (a) DFDA. (b) Bended DFDA. (c) MFDA.

Fig. 3. Configuration and decomposition of DFDA.

the advantages of wide bandwidth, two upper radiation nulls, and EM transparent characteristics in HB. To have a deeper insight into the proposed antenna, the working principle of the MFDA is interpreted in the following paragraphs.

For $\pm 45°$ polarization feeding ports, the proposed MFDA can be assumed as a combination of two bended DFDA as illustrated in Fig. 2. Thus, to have a deeper insight into MFDA, the working principle of DFDA is analyzed first. As shown in Fig. 3, the currents on the DFDA can be decomposed into two distinct modes: a TL mode and a dipole antenna (DA) mode.

For the TL Mode, the conductors are driven by two generators with equal magnitude ($V/2$) and 180° phase difference. The current on the conductors is I_{TL}. By dividing the TL mode into two identical loaded TLs with length $L_{T2}/2$ at the central plane, the impedance of each part can be derived from

$$Z_{TL2} = Z_c \frac{Z_{FD} + jZ_c\tan\left(k\frac{L_{T2}}{2}\right)}{Z_c + jZ_{FD}\tan\left(k\frac{L_{T2}}{2}\right)} \qquad (1)$$

where Z_c is the characteristic impedance of two-wire TLs. Z_{FD} is the impedance of the folded-DA. k is the propagation constant, and L_{T2} is the length of the TL. Z_c can be calculated by substituting W, and $g = G_2$ into the following equations [34]:

$$Z_c = 120\pi \frac{K(x)}{K(x')} \qquad (2)$$

$$x^2 + x'^2 = 1 \qquad (3)$$

$$x = \frac{g}{g + 2W} \qquad (4)$$

where $K(x)$ is the complete elliptic function of the first kind. The impedance of the folded-DA [35] is

$$Z_{FD} = \frac{4Z_{DA1}Z_{TL1}}{2Z_{DA1} + Z_{TL1}} \qquad (5)$$

where Z_{TL1} is the impedances of its TL mode

$$Z_{TL1} = jZ_c\tan\left(k\frac{L_{T1}}{2}\right). \qquad (6)$$

By substituting $l = L_{T1}$ into (7), the impedance of equivalent DA mode Z_{DA1} can be obtained [35]

$$Z_{DA} = \frac{R_{DA} + jX_{DA}}{sin^2(kl)} \qquad (7)$$

where R_{DA1} and X_{DA1} can be expressed as

$$R_{DA} = \frac{\eta}{2\pi}\left\{ \begin{array}{l} C + \ln(kl) - C_i(kl) \\ \frac{1}{2}sin(kl)[S_i(2kl) - 2S_i(kl)] \\ +\frac{1}{2}cos(kl)\left[\begin{array}{l} C + \ln\left(k\frac{l}{2}\right) + C_i(2kl) \\ -2C_i(kl) \end{array} \right] \end{array} \right\} \qquad (8)$$

$$X_{DA} = \frac{\eta}{4\pi}\left\{ \begin{array}{l} 2S_i(kl) + cos(kl)[2S_i(kl) - S_i(2kl)] \\ -sin(kl)\left[2C_i(kl) - C_i(2kl) - C_i\left(2k\frac{a_E}{l}\right)\right] \end{array} \right\} \qquad (9)$$

where a_E represents the equivalent radius of the dipole and, it can be calculated by substituting $g = G_1$ into (9)

$$a_E = \sqrt[2]{\frac{W}{4}\left(\frac{g + W}{2} + \sqrt[2]{\left(\frac{g + W}{2}\right)^2 - \left(\frac{W}{4}\right)^2}\right)}. \qquad (10)$$

Therefore, the current I_{TL} can be calculated by using

$$I_{TL} = \frac{V/2}{Z_{TL2}}. \qquad (11)$$

For the DA mode, the conductors are driven by two identical generators with equal magnitude ($V/2$). It can be equivalent to a DA with an equivalent radius (a_E) and equivalent length L_E. The equivalent length L_E can be obtained by using the method in [36]. The impedance of DA Mode Z_{DA2} can be calculated by substituting W, $l = L_E$, $g = G_2$ into (7)–(10). The current for the DA mode is given by

$$I_{DA} = \frac{V/2}{Z_{DA2}}. \qquad (12)$$

Thus, the total current on the DFDA I_{IN} is given by

$$I_{IN} = I_{TL} + \frac{I_{DA}}{2} = \frac{V(2Z_{DA2} + Z_{TL2})}{4Z_{DA2}Z_{TL2}}. \qquad (13)$$

The impedance of DFDA is given by

$$Z_{IN} = \frac{4Z_{DA2}Z_{TL2}}{2Z_{DA2} + Z_{TL2}}. \qquad (14)$$

Based on the analysis above, the input impedance of the DFDA is calculated by using MATLAB. As shown in Fig. 4, the calculated results agree well with the simulated results. Thus, the proposed TL and DA model can be used to accurately analyze the impedance characteristic of DFDA.
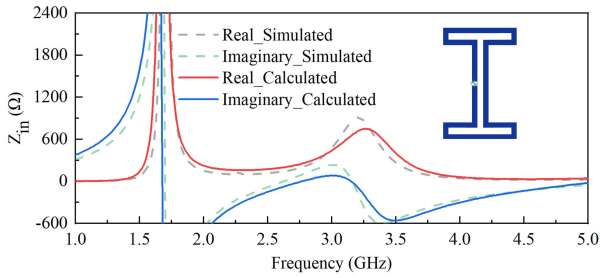
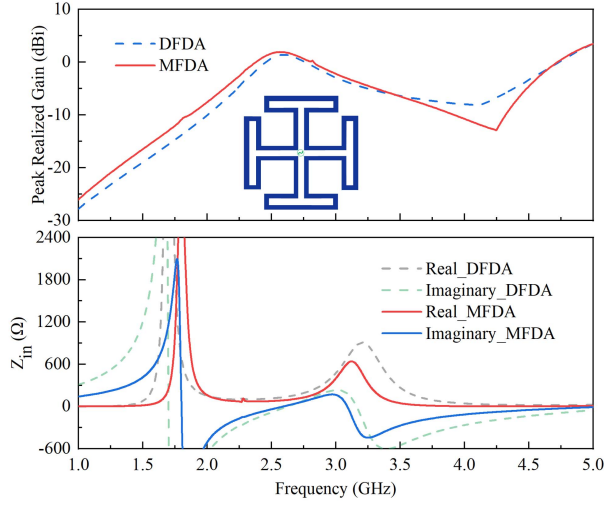Fig. 4. Calculated and simulated input impedances of DFDA without substrate.

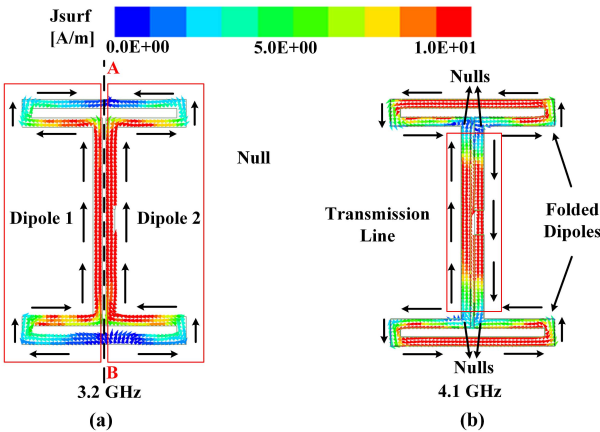Fig. 5. Simulated peak realized gains and input impedances of the DFDA and MFDA.

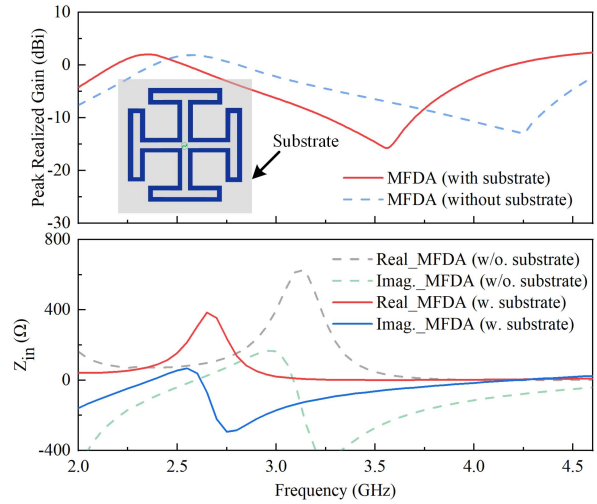Fig. 6. Simulated current distributions of the DFDA at (a) 3.2 GHz and (b) 4.1 GHz.

Fig. 7. Simulated peak realized gains and input impedances of the MFDA with and without substrate.

current distribution of the DFDA in Fig. 6(b) demonstrates that the TL mode is the dominant mode at 4.1 GHz. At this frequency, the currents on the central part of the DFDA flow in opposite directions. It can be seen as a section of TL. The current distribution on the two folded dipoles shows that they work under their first-order mode [37]. As mentioned in [37], the input resistance of the first-order mode of the linear folded dipole is very large and close to infinite. So, they can be equivalent to open circuits. Therefore, no power will be radiated into the free space at this frequency. This can also be verified by the current distribution in Fig. 6(b). It can be seen that there are four current nulls at the inputs of the folded dipoles. All the power will be reflected back to the source at this frequency. Thus, a radiation null appears at this frequency. Then, by combining two bended DFDA, an MFDA is obtained. It can be seen in Fig. 5 that the resonant frequencies of the radiative mode and radiation null of the MFDA are almost the same as the DFDA.

It is worth noting that the influences of the substrate on the DFDA and MFDA are not included in the calculation and simulation presented above. To facilitate fabrication, a Rogers 4003 substrate with a thickness of 0.508 mm is introduced to support the MFDA. As given in Fig. 7, the resonant mode and radiation null shift toward a lower frequency band after introducing the substrate.

In the presented antenna, four parasitic RLs are placed under the MFDA to further enhance the out-of-band rejection level of the higher frequency band. As shown in Fig. 8, the first radiation null shifts toward a lower frequency after introducing the parasitic loops, and the input impedance of the radiative resonant mode is reduced. Furthermore, a new radiation null (second radiation null) is introduced at 4.5 GHz. To interpret the working principle of the second radiation null, the simulated current distribution of the antenna at 4.5 GHz is given in Fig. 9. It can be observed that the current distributions on the parasitic RLs are opposite to the current distributions on the MFDA. Thus, the radiation power in the far-field zone is

As shown in Fig. 5, a radiative resonant mode and radiation null appears at 3.2 and 4.1 GHz, respectively. To understand their working principles, the simulated current distributions are given in Fig. 6. It can be seen from Fig. 6(a) that the DA mode plays a dominant role at 3.2 GHz in effective radiation. Owing to the currents flowing in the same direction on both sides, the symmetrical plane (A-B) can be equivalent to an open circuit, and the currents flow in the same direction on both sides. The
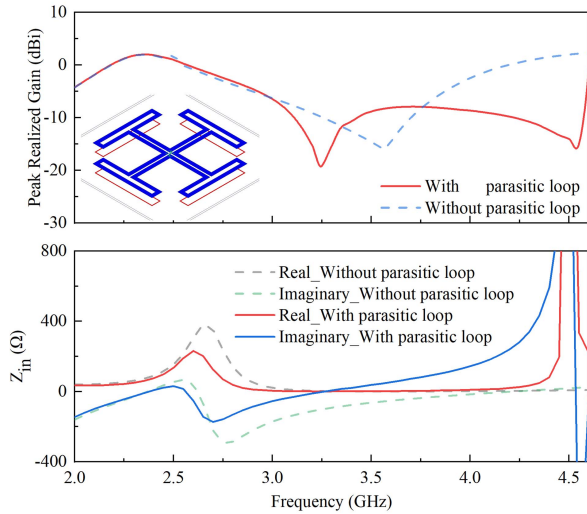
Fig. 8.   Simulated peak realized gains and input impedances of the MFDA with and without parasitic loops.
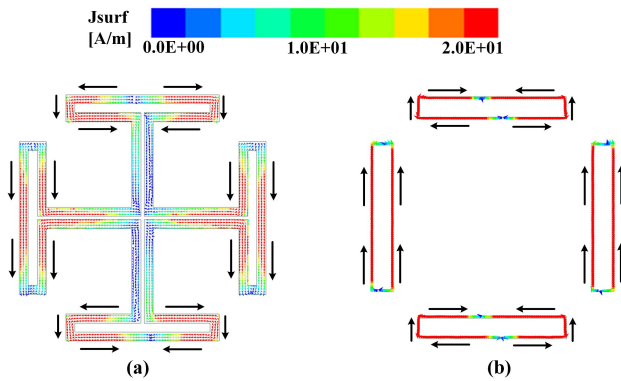

Fig. 9.   Simulated current distributions of the antenna on (a) MFDA and (b) parasitic RLs at 4.5 GHz.
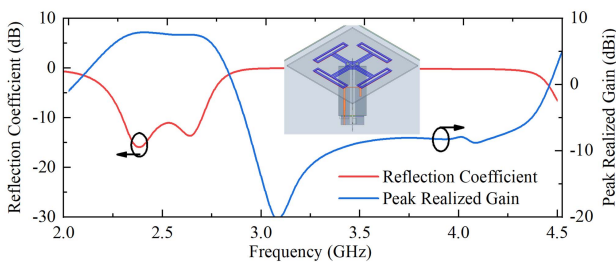

Fig. 10.   Configuration and simulated results of the proposed LB element.

canceled by each other. Due to all the power being reflected back to the source, a new radiation null is obtained at this frequency.

Then, by feeding the antenna using two orthogonal printed baluns, a ±45° dual-polarization antenna with a compact size and upper out-of-band rejection is achieved. The simulated peak realized gain and reflection coefficient are shown in Fig. 10. The proposed antenna can cover the frequency range of 2.3–2.7 GHz. Besides, the out-of-band rejection level is higher than 16 dB.
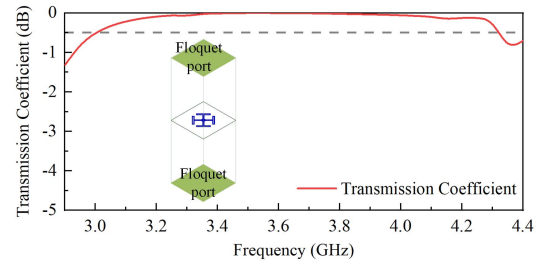

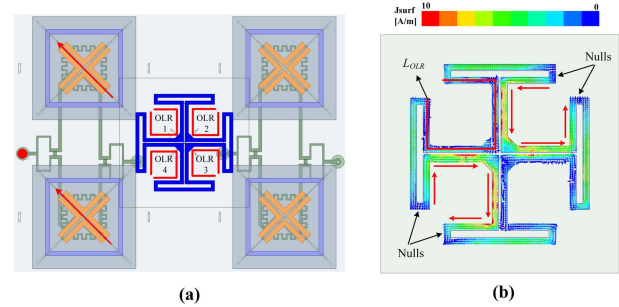Fig. 11.   Simulated transmission coefficient of the proposed radiator.

Fig. 12.   (a) Configuration of the dual-band array and (b) simulated current distribution on the radiator at 3.6 GHz when the HB sub-array is excited.

Apart from the advantages mentioned above, the proposed antenna also has an EM transparent characteristic at a higher frequency band. The simulated transmission coefficient of the LB radiator is shown in Fig. 11. It can be observed that the simulated transmission coefficient of the proposed radiator is higher than −0.5 dB from 3.0 to 4.3 GHz. Due to the high transmission coefficient level, the proposed LB antenna has little influence on the radiation patterns of the HB antennas.

As shown in Fig. 12(a), the LB radiator has four open-loop resonators (OLRs). Each OLR can be equivalent to an LC parallel resonance circuit, working as a bandpass surface, which is transparent to the wave radiated from the HB antenna. As shown in Fig. 12(b), when a −45° polarized incident EM wave irradiates the LB radiator, the OLR 2 and 4 are excited and play an important role in transmitting the wave through them. Due to the symmetry of the radiator, it will be the same phenomenon that the OLR 1 and 3 will be excited when +45° polarized incident EM wave irradiates on the LB radiator. As a result, the HB EM wave can be transmitted through the LB radiator without being affected. Therefore, the LB antenna can be seen as an EM transparent antenna for the HB antennas. The resonant frequency of the OLRs (central frequency of the EM transparent band) can be calculated by using

$$f_{OLR} \approx \frac{c}{2L_{OLR}} \tag{15}$$

where c is the speed of the light in free space and L_{OLR} is the length of the OLR.

In this section, the DFDA is firstly analyzed by using TL and DA modes. The calculated input impedance of the DFDA agrees well with the simulated one. Based on the analysis, the working mode of the DFDA can be divided into DA and TL modes. Under the TL mode, the DFDA will transmit the EM

wave into free space. Under the TL mode, all the power will be reflected back to the source. Therefore, by combining two bended DFDA and introducing four parasitic loops, an LB antenna with compact size and good performance can be obtained. Moreover, the proposed antenna has little influence on the radiation patterns of the HB array owing to the EM transparent characteristic. These are very important advantages in the design of dual-band dual-polarized base station array antenna.

B. HB Element

Having an HB element with a good out-of-band suppression level in a lower frequency band is critical in the design of a dual-band base station array antenna with low couplings. In this section, an HB element with a high suppression level and sharp cut-off in the lower frequency band is achieved by using MLL, RL, and VSS.

The configurations and dimensions of the proposed HB antenna are given in Fig. 13. It can be seen that all conductors of the proposed HB element are printed on three Rogers RO4003 substrates with a thickness of 0.508, 0.305, and 0.508 mm, respectively. The VSS and MLL are printed on the upper and lower layers of substrate 1. The RL is printed on the lower layer of Substrate 2. The dipole arms of this antenna are vertically printed and connected to the baluns.

The simulated peak realized gain and reflection coefficient are shown in Fig. 14. It can be seen that the proposed HB element has a wide impedance bandwidth of 42.5% (3.0–4.62 GHz), a stable peak realized gain of 8.9 dBi, and a good out-of-band rejection level of 17 dB. Besides, the proposed antenna obtains a high RoR of 242.9 dB/GHz ($f_{20\,dB}$ is 2.87 GHz, $f_{3\,dB}$ is 2.94 GHz), which is crucial in the design of a multiband array antenna with a low-frequency ratio. The RoR is calculated by using [38]

$$RoR = \frac{20 - 3}{|f_{20\,dB} - f_{3\,dB}|} \quad (16)$$

where $f_{3\,dB}$ and $f_{20\,dB}$ are the frequencies where the average peak realized gain drops by 3 and 20 dB, respectively.

To better demonstrate the working principle of the proposed HB element, three reference antennas are given in Fig. 15. Antenna 1 is a vertically printed crossed DA. By introducing an RL under the arms of Antenna 1, first radiation null and a new resonant mode can be obtained to suppress the out-of-band radiation and expand the impedance bandwidth [39]. To further enhance the RoR, an MLL is placed above the arms of the crossed dipoles in Antenna 2. After introducing the MLL, a new radiation null appears at the in-band of the antenna. Finally, four VSS are introduced above the MLL to shift the second radiation null toward the lower frequency band.

Fig. 16 shows the simulated results of the reference antennas and proposed HB element. It can be observed that the out-of-band rejection of the Antenna 1 can be effectively developed by introducing the RL. Besides, the bandwidth is increased due to the new resonant mode. Then, by introducing an MLL above the dipole arms, the second radiation null is realized at 3.5 GHz.
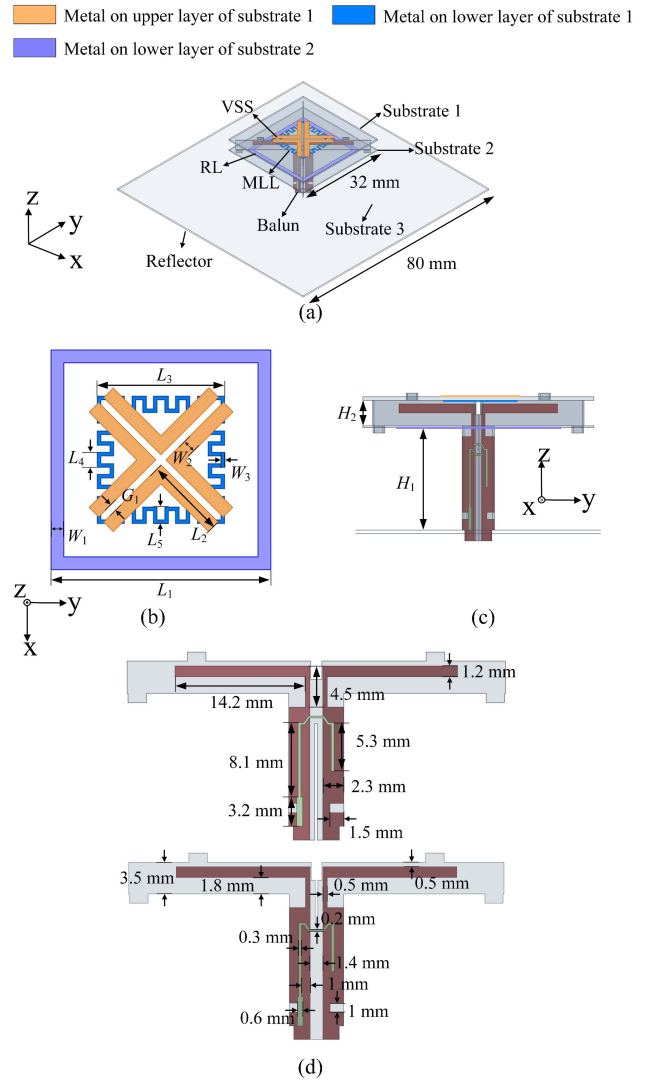

Fig. 13. Configuration of the proposed HB antenna. (a) Three-dimensional view, (b) top view, (c) side view, and (d) balun and dipole arms. Dimensions are $L_1 = 24.2$, $L_2 = 8.9$, $L_3 = 22.8$, $L_4 = 1.6$, $L_5 = 1.8$, $W_1 = 1.4$, $W_2 = 1.5$, $W_3 = 0.4$, $G_1 = 0.8$, $H_1 = 14.2$, and $H_2 = 3.5$ (unit: millimeter).
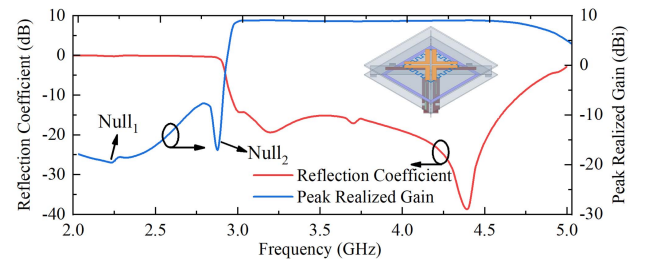

Fig. 14. Configuration and simulated results of the HB element.

To interpret the working principle of the second radiation null, the equivalent circuit of MLL is given in Fig. 17. For the $-45°$ polarization, the MLL can be divided into two identical parts (Parts 1 and 2). Each part has two meander line (ML) elements. One is horizontally printed; another is vertically printed. For horizontal electric field (E_h), ML_1 can
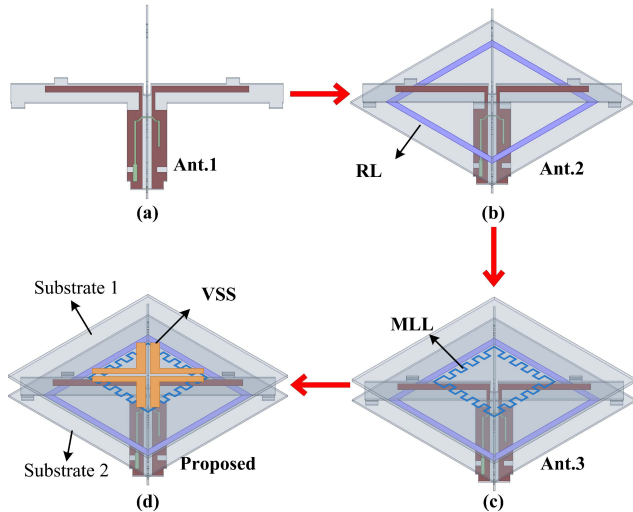
Fig. 15.   Evolution of the HB element. (a) Crossed dipoles. (b) With rectangular loop. (c) With meander line loop. (d) Proposed antenna.
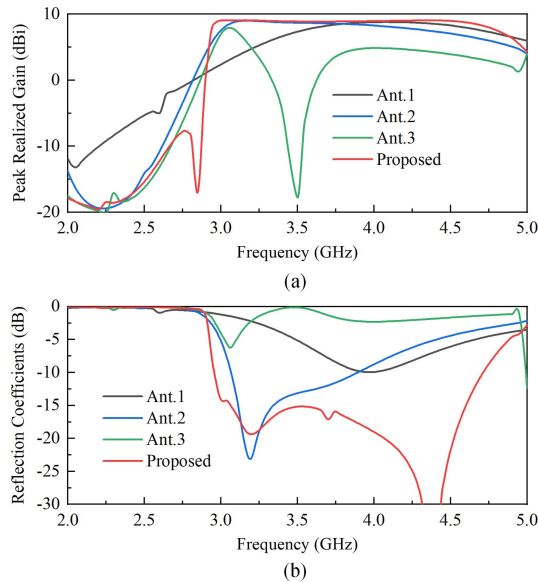

Fig. 16.   Simulated (a) normalized peak realized gain, and (b) reflection coefficients of the proposed HB element and reference antennas.

be equivalent to a shunt inductance over an equivalent TL, and ML_2 can be equivalent to a shunt capacitance. For vertical electric field (E_v), ML_1 will act like a shunt capacitance and ML_2 will act like a shunt inductance [40]. Therefore, for the electric field with a $-45°$ angle, Part 1 can be equivalent to a series L-C resonator. The MLL acts like a band-stop filter. The resonant frequency of the MLL can be calculated by employing

$$f_{null} = \frac{1}{2\pi\sqrt{L_1 C_1}}. \tag{17}$$

To shift the second radiation null out of the operating band of the HB element, four parasitic VSSs are introduced above the MLL. It can be observed from Fig. 16 that the second radiation null is moved from 3.5 to 2.9 GHz without
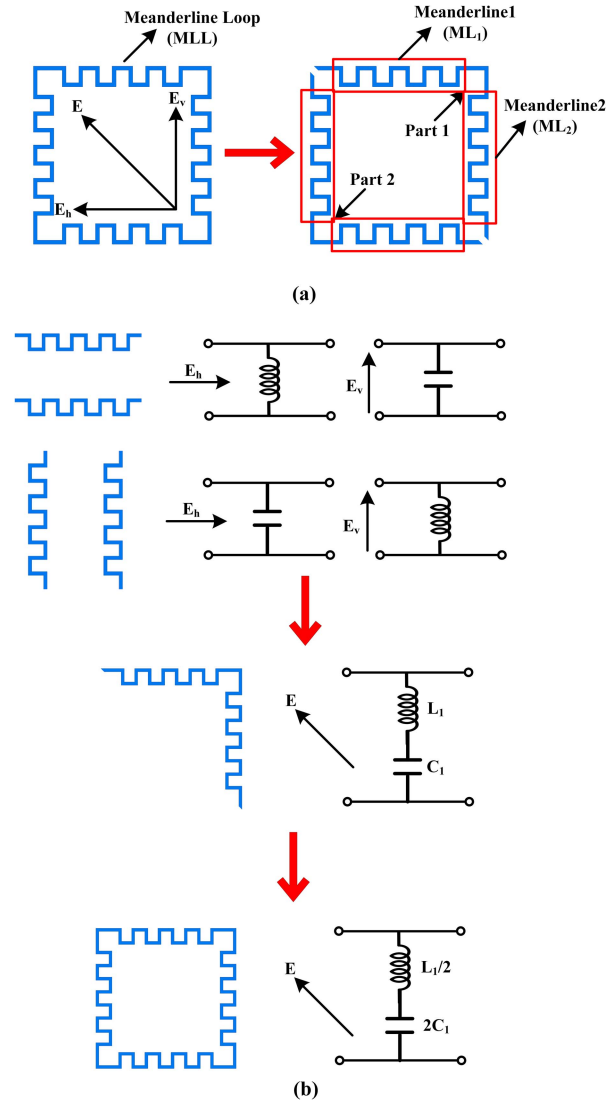

Fig. 17.   Equivalent circuits of the MLL. (a) Decomposition. (b) Equivalent circuits of the MLL.

increasing the aperture of the antenna after introducing the VSSs. Besides, the *RoR* increases from 45.9 to 242.9 dB/GHz.

Overall, in this section, a novel HB element with high *RoR* is proposed by combining the RL, MLL, and VSS. Firstly, an RL is placed under the arms of the crossed dipoles to obtain the first radiation null and excite a new resonant mode. Then, to enhance the *RoR* and out-of-band rejection level, an MLL is printed above the dipole arms. The working principle of the MLL is then analyzed. By introducing four VSSs, the second radiation null can be shifted toward the lower frequency band. As a result, an HB element with wide impedance bandwidth and a high *RoR* is achieved in this work.

III. DUAL-BAND DUAL-POLARIZED ARRAY

Based on the LB and HB elements designed above, a dual-band dual-polarized array antenna is realized in this section. As shown in Fig. 18, the size of the ground plane is 164 × 142 mm. The LB element is placed in the center of the ground plane and above the HB elements. The four HB elements
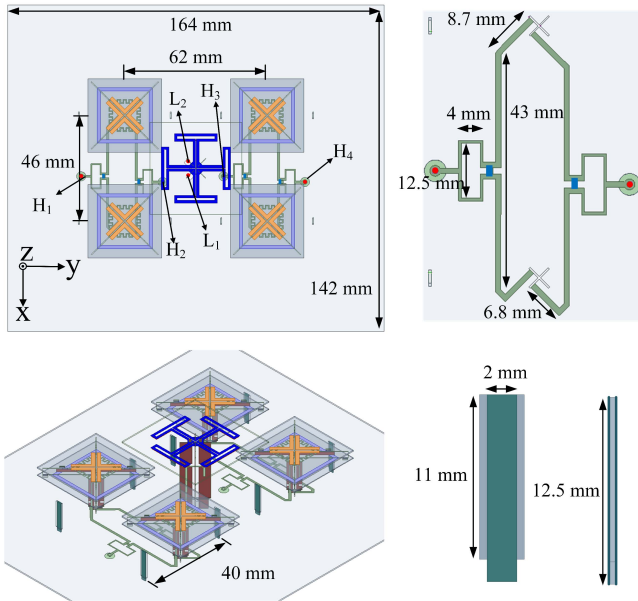
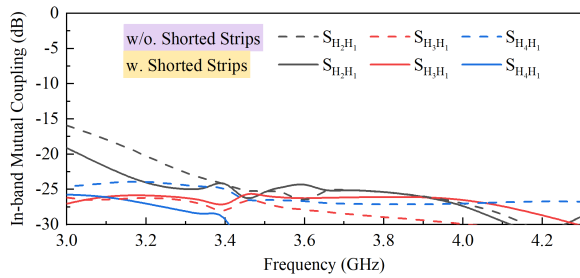Fig. 18. Configuration of the dual-band dual-polarized array antenna.

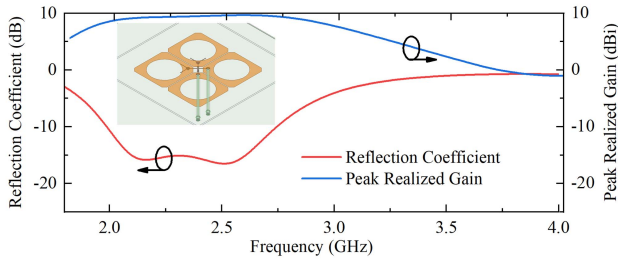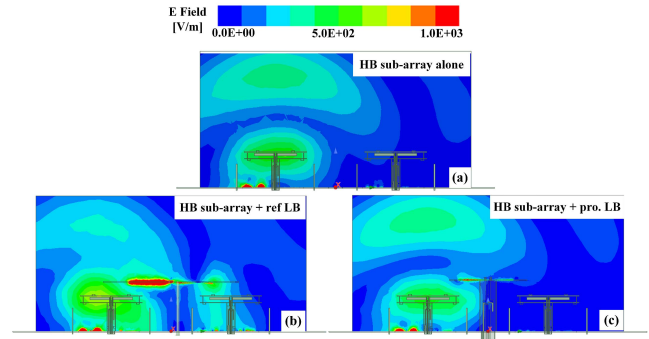Fig. 19. Simulated isolations of the HB sub-arrays with and without shorted strips.

Fig. 20. Configuration and simulated results of the reference LB element.

Fig. 21. Simulated E-Field distributions of the HB sub-array (port H_1 excited) at 3.6 GHz under different configurations. (a) HB sub-array alone, (b) HB sub-array + reference LB element, and (c) HB sub-array + MFDA.
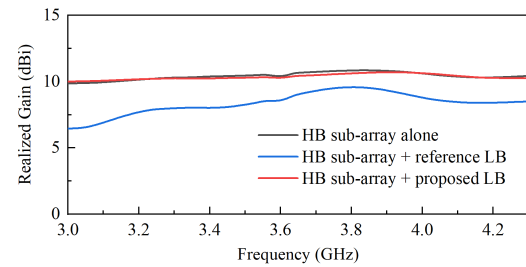
Fig. 22. Simulated peak realized gains of the HB sub-array (port H_1 excited) under different configurations.

are divided into two columns. Elements in each column are fed by two Wilkinson power dividers. The distances between the elements along the x-axis and y-axis are 46 and 62 mm, respectively.

It should be noted that eight shorted strips are introduced to reduce the coupling between the input ports of the HB elements. Fig. 19 shows the simulated reflection coefficients of the proposed HB array with and without shorted strips. As can be seen, the isolation between ports H_1 and H_2 increased from 15 to 19 dB after introducing the shorted strips. It demonstrates that the shorted strips play an important role in reducing the mutual couplings between the HB sub-arrays.

To verify the performance of the proposed antenna, a reference dual-band array antenna is designed by using the most common crossed dipole elements. The configurations of these two dual-band array antennas are the same except for the LB elements. The configuration and simulated results of the reference LB element are shown in Fig. 20. The E-field distributions of the HB sub-array are given in Fig. 21. It can be observed that the HB sub-array is severely blocked by the reference LB antenna when using the ordinary dual-polarized crossed DA. The E-field of the HB sub-array is disturbed and reflected. As a result, the radiation performance of the HB sub-array will be seriously distorted. The simulated peak realized gains of the HB sub-array under different configurations are shown in Fig. 22. It can be seen the peak realized gain of the HB sub-array drops 3.6 dB at 3 GHz after introducing the reference LB element, which is unacceptable in dual-band base station application. However, by comparing the E-field distributions in Fig. 21(a) and (c), it is not difficult to find that the proposed LB element has little influence on the radiation performance of the HB sub-array and it can be seen as an EM transparent antenna at this frequency. Besides, as depicted in Fig. 22, the peak realized gain of the HB sub-array keeps almost unchanged after introducing the proposed LB element. The max gain difference is only 0.2 dB.

The comparison between the radiation patterns of the HB sub-array (without LB element, with reference LB element, and with proposed LB element) is given in Fig. 23. As depicted, the reference LB element has a great influence on the radiation patterns of the HB sub-array. When using the
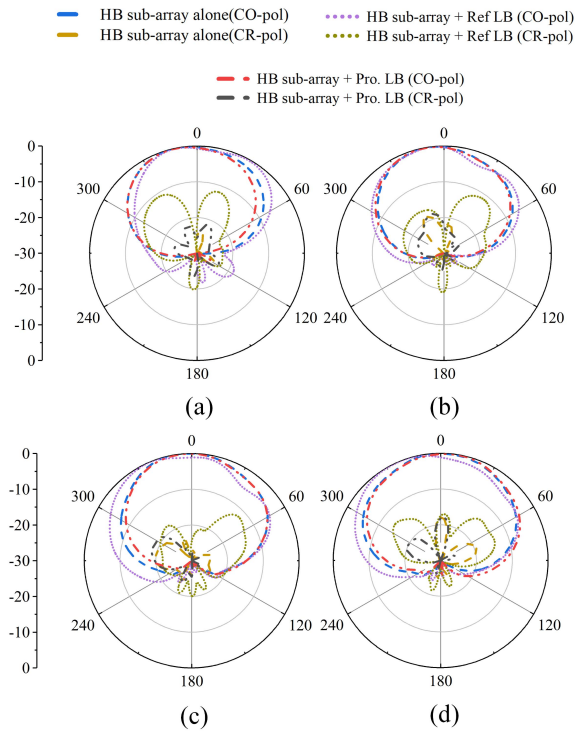
Fig. 23. Simulated normalized radiation patterns of the HB sub-array (port H_1 excited) in the horizontal plane under different configurations at (a) 3.0 GHz, (b) 3.6 GHz, (c) 4.0 GHz, and (d) 4.3 GHz.
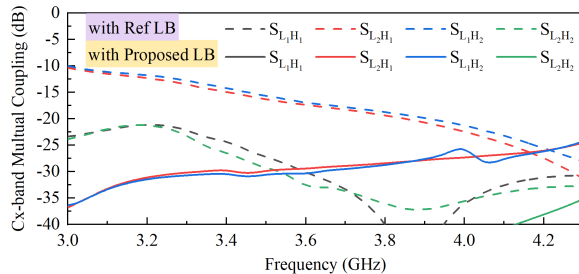

Fig. 24. Simulated cross-band coupling of the proposed array antenna and the reference array antenna.

ordinary LB element, both co-polarized and cross-polarized radiation patterns of the HB sub-array deteriorate. However, by replacing it with the proposed LB element, the radiation patterns of the HB sub-array remain almost unchanged. This is highly desirable for present base station applications.

Besides, due to the good filtering performance of the proposed LB element, the cross-band coupling of the proposed dual-band array antenna is much lower than the reference one, as depicted in Fig. 24. The simulated isolations between the HB sub-array and the reference LB element are higher than 10 dB from 3 to 4.3 GHz. However, in the proposed dual-band array antenna, the isolations between the HB sub-array and the proposed LB element are higher than 24 dB within the same frequency band, which shows a significant improvement in the array design.

In this section, based on the proposed LB and HB elements, a novel dual-band dual-polarized base station array
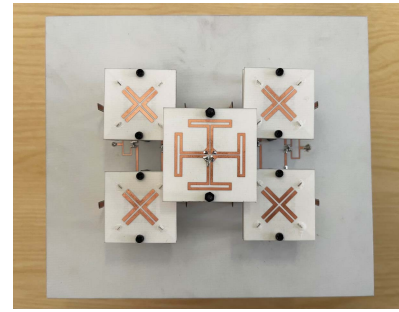
Fig. 25. Fabricated prototype of the dual-band array antenna.
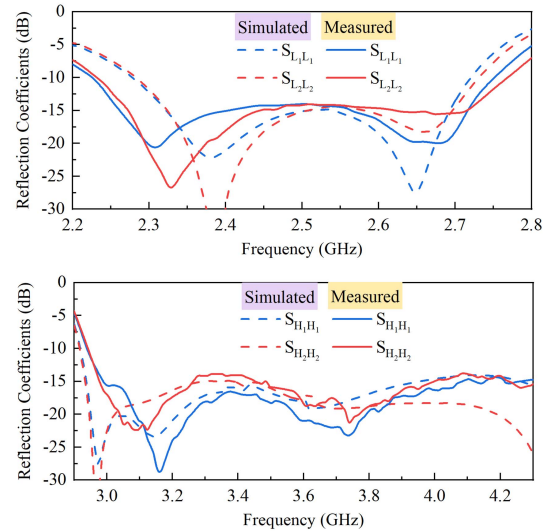
Fig. 26. Measured and simulated reflection coefficients of the dual-band array antenna.

antenna is achieved. To validate the advantages of the proposed antenna, a reference dual-band array antenna is designed. It is worth noting that the only difference between these two dual-band array antennas is the structure of the LB element. Simulated results demonstrate the proposed LB element has little influence on the radiation performance of the HB array. Furthermore, the proposed dual-band array antenna shows a significant improvement in cross-band isolation.

IV. RESULTS AND DISCUSSION

For verification, a prototype of the proposed dual-band dual-polarized array antenna is fabricated as shown in Fig. 25. The measured S-parameters are obtained by using the R&S[1]ZVL vector network analyzer. The far-field results are obtained in the anechoic chamber at the University of Kent. Fig. 26 shows the measured and simulated reflection coefficients of the LB element and HB array in the dual-band array. According to the measured results, the proposed LB element has an impedance bandwidth of 18.8% (2.26–2.73 GHz) with a reflection coefficient <-14 dB. For the HB sub-array, the measured and simulated results are in reasonable agreement with each other. The measured results indicate that the proposed HB

---

[1]Registered trademark.

Fig. 27. Measured and simulated mutual couplings of the dual-band array antenna.

Fig. 28. Measured and simulated realized gain of the dual-band array antenna.

Fig. 29. Measured and simulated normalized radiation patterns of the LB element in the horizontal plane at (a) 2.3 GHz and (b) 2.7 GHz.

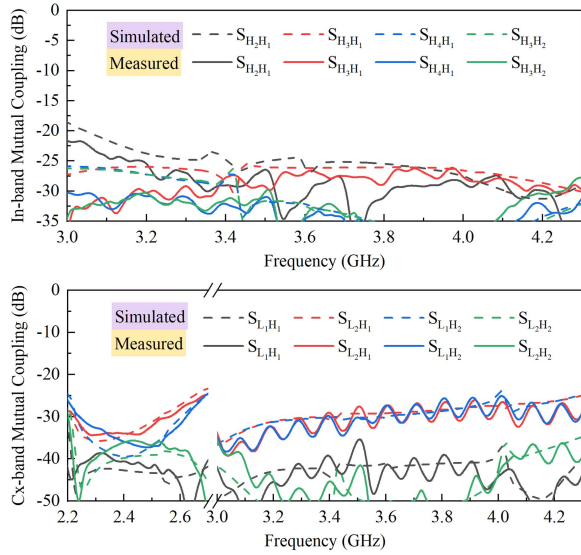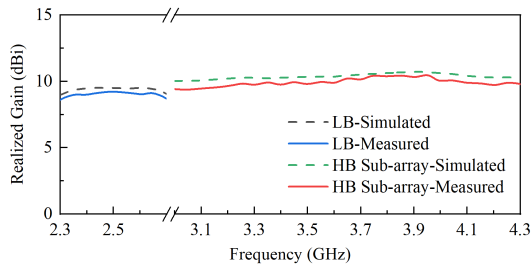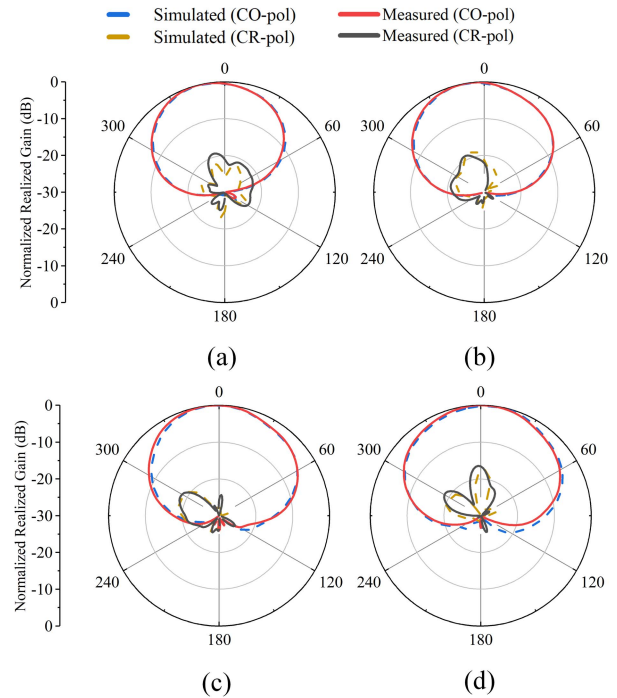Fig. 30. Measured and simulated normalized radiation patterns of the HB sub-array in the horizontal plane at (a) 3.0 GHz, (b) 3.6 GHz, (c) 4.0 GHz, and (d) 4.3 GHz.

sub-array realizes a wide bandwidth of 36% (2.98–4.3 GHz) for reflection coefficients lower than −14 dB.

Fig. 27 exhibits the measured and simulated in-band and cross-band mutual couplings of the proposed dual-band array antenna. It can be observed from the measured results that the in-band isolations between port H_1 and port H_2 are higher than 22 dB. The isolations between other ports of the HB sub-arrays are higher than 25 dB. Due to the good filtering performance of the proposed LB and HB element, the cross-band mutual couplings between the input ports of the LB element and HB sub-arrays are all higher than 25 dB.

The measured and simulated broadside realized gains of the proposed dual-band array antenna are shown in Fig. 28. For the LB element, an average measured realized gain of 8.9 dBi is achieved within the operating band. It is slightly lower than the simulated value of 9.2 dBi because of the loss of the cables and test environment. For the HB sub-array, the measured realized gains distribute between 9.4 and 10.5 dBi while the simulated one is all within the range of 10–10.7 dBi. The ripples in the operating band, as well as the slight gain variation between the measured and simulated curves, can be attributed to the loss of the test equipment and fabrication error.

The measured and simulated normalized radiation patterns of the LB element and HB sub-array in the horizontal

plane at different frequencies are shown in Figs. 29 and 30, respectively. As can be observed, the measured results are in good agreement with the simulated results. The measured cross-polarization levels of the LB element and HB array are 20 and 21 dB lower than their co-polarization levels in broadside.

The comparisons between the proposed antenna and recently published dual-band dual-polarized array antennas are shown in Table I. By introducing the FSS structure [20], [21] and etching the HB elements in the dipole arms of the LB element [23], three dual-band arrays with high cross-band isolations are developed. However, the frequency ratios of these antennas are larger than 4.3. In [24] and [25], two interleaved shared-aperture dual-band array antennas are realized by introducing branches on the radiator of the LB

TABLE I
COMPARISON OF THE PREVIOUSLY PRESENTED DUAL-BAND DUAL-POLARIZED ARRAY ANTENNAS

Ref.	Elements Arrangement	HB (GHz); $|S_{11}|$ (dB)	LB (GHz); $|S_{11}|$ (dB)	Freq. Ratio	Gain of LB element (dBi)	Cx-band Iso. (dB)	In-band Iso. (dB)	HB Elements Spacing (λ_{HL})
[20]	2×2 HB above LB	3.5-4.9 (33%); -14	0.69-0.96 (33%); -10	5.09	8.7 ± 1	24	21	0.73 × 0.73
[21]	2×2 HB above LB	3.4-3.7 (8%); -10	0.69-0.96 (33%); -10	4.3	7.4 ± 0.3	32	20	0.54 × 0.54
[23]	Coplanar 2×2 HB and LB	3.3-3.8 (14%); -14	0.69-0.96 (33%); -14	4.3	8.7 ± 0.6	29	25	0.92 × 0.92
[24]	2×2 HB under LB	3.4-3.8 (11%); -14	0.69-0.96 (33%); -14	4.36	6.8 ± /	/	/	0.51 × 0.68
[25]	2×2 HB under LB	1.7-2.7 (46%); -14	0.69-0.96 (33%); -14	2.7	7.6 ± 0.6	19	19	/
[26]	2×2 HB under LB	1.71-2.28 (28%); -14	0.82-1.0 (20%); -10	2.19	6.5 ± 0.5	/	/	0.57 × 0.86
[27]	2×2 HB under LB	3.3-3.8 (14%); -11	1.71-2.17 (24%); -12	1.8	7.9 ± 0.5	20	20	0.5 × 0.66
[29]	2×2 HB under LB	3.3-3.8 (14%); -12	1.8-2.7 (40%); -10	1.58	8.6 ± 1.3	20	20	0.47 × 0.69
[30]	A LB stacked on a HB	3.3-3.8 (14%); -14	2.3-2.7 (16%); -14	1.42	9.1 ± 0.3	/	/	/
This Work	**2×2 HB under LB**	**3.0-4.3 (36%); -14**	**2.26-2.73 (19%); -14**	**1.46**	**8.9 ± 0.3**	**25**	**22**	**0.46 × 0.62**

* λ_{HL}, and λ_{LL} are the wavelength at the lowest operating frequency in free space of higher band and lower band, respectively. Iso. represents isolation.

element. However, the frequency ratios of these two dual-band array antennas are nearly twice of the proposed antenna. Four dual-band array antennas with frequency ratios smaller than 2 are developed in [27], [29], [30], and [31]. Although the LB element in [27], [29], and [30] obtain a wider impedance bandwidth than the proposed one, their wave-transparent bands are much narrower than our work. Besides, the proposed dual-band array antenna realizes a smaller frequency ratio, a higher gain, and higher isolation than the designs in [27] and [30]. LB element in [31] achieves a high realized gain of 9.1 dBi, however, the impedance bandwidths of both LB and HB in this design are narrower than in our work.

V. CONCLUSION

Two new methods are proposed in this article to design the LB and HB elements in the dual-band dual-polarized array antenna. Based on the proposed method, a novel low-scattering low-pass LB element and a novel high-*RoR* high-pass HB element are able to realize. By combining these two high-performance elements and introducing eight shorted strips, a novel shared-aperture dual-band dual-polarized array antenna with wide impedance bandwidths, high in-band and cross-band isolation, and low cross-band scattering can be realized. The measured results show that the proposed array antenna works at 2.26–2.73 and 2.98–4.3 GHz with reflection coefficients lower than −14 dB. The in-band and cross-band isolations of the proposed array antenna are higher than 22 and 25 dB, respectively. Such a high-performance dual-band dual-polarized array antenna is a good candidate for present base station applications.

REFERENCES

[1] H. Zhai, Y. Zang, and L. Li, "A low-profile dual-polarized high-isolation MIMO antenna arrays for wideband base-station applications," *IEEE Trans. Antennas Propag.*, vol. 66, no. 1, pp. 191–202, Jan. 2018.

[2] J. Yin, Y. Jia, S. Yang, and H. Zhai, "Design of a composite decoupling structure for dual-band dual-polarized base station array," *IEEE Antennas Wireless Propag. Lett.*, vol. 21, no. 7, pp. 1408–1412, Jul. 2022, doi: 10.1109/LAWP.2022.3170081.

[3] Y. He, Z. Pan, X. Cheng, J. Qiao, and M. M. Tentzeris, "A novel dual-band, dual-polarized, miniaturized and low-profile base station antenna," *IEEE Trans. Antennas Propag.*, vol. 63, no. 12, pp. 5399–5408, Dec. 2015.

[4] H. Huang, Y. Liu, and S. Gong, "A novel dual-broadband and dual-polarized antenna for 2G/3G/LTE base stations," *IEEE Trans. Antennas Propag.*, vol. 64, no. 9, pp. 4113–4118, Sep. 2016.

[5] B. Liu, Y. Da, X. Chen, and A. A. Kishk, "Hybrid decoupling structure based on neutralization and partition schemes for compact large-scale base station arrays," *IEEE Antennas Wireless Propag. Lett.*, vol. 21, no. 2, pp. 267–271, Feb. 2022.

[6] M. Li, Q. Li, B. Wang, C. Zhou, and S. Cheung, "A miniaturized dual-band base station array antenna using band notch dipole antenna elements and AMC reflectors," *IEEE Trans. Antennas Propag.*, vol. 66, no. 6, pp. 3189–3194, Jun. 2018.

[7] Y. Zhang, X. Y. Zhang, L.-H. Ye, and Y.-M. Pan, "Dual-band base station array using filtering antenna elements for mutual coupling suppression," *IEEE Trans. Antennas Propag.*, vol. 64, no. 8, pp. 3423–3430, Aug. 2016.

[8] M. Li, R. Wang, J. M. Yasir, and L. Jiang, "A miniaturized dual-band dual-polarized band-notched slot antenna array with high isolation for base station applications," *IEEE Trans. Antennas Propag.*, vol. 68, no. 2, pp. 795–804, Feb. 2020.

[9] D. Wen, Y. F. Cao, Y. M. Pan, Z. X. Chen, and X. Y. Zhang, "Compact dual-band dual-polarized base-station antenna array with a small frequency ratio using filtering elements," *IEEE Access*, vol. 7, pp. 127800–127808, 2019.

[10] X.-Y. Zhang, D. Xue, L.-H. Ye, Y.-M. Pan, and Y. Zhang, "Compact dual-band dual-polarized interleaved two-beam array with stable radiation pattern based on filtering elements," *IEEE Trans. Antennas Propag.*, vol. 65, no. 9, pp. 4566–4575, Sep. 2017.

[11] X. Liu et al., "A compact dual-polarized filtering antenna with steep cut-off for base-station applications," *IEEE Trans. Antennas Propag.*, vol. 70, no. 7, pp. 5941–5946, Jul. 2022, doi: 10.1109/TAP.2022.3161280.

[12] C.-X. Mao, S. Gao, Y. Wang, Q. Luo, and Q.-X. Chu, "A shared-aperture dual-band dual-polarized filtering-antenna-array with improved frequency response," *IEEE Trans. Antennas Propag.*, vol. 65, no. 4, pp. 1836–1844, Apr. 2017.

[13] Y.-M. Zhang, S. Zhang, J.-L. Li, and G. F. Pedersen, "A transmission-line-based decoupling method for MIMO antenna arrays," *IEEE Trans. Antennas Propag.*, vol. 67, no. 5, pp. 3117–3131, May 2019.

[14] Y.-M. Zhang, S. Zhang, J.-L. Li, and G. F. Pedersen, "A wavetrap-based decoupling technique for 45° polarized MIMO antenna arrays," *IEEE Trans. Antennas Propag.*, vol. 68, no. 3, pp. 2148–2157, Mar. 2020.

[15] H. Lin, W. Yu, F. Deng, B. Liao, and R. Tang, "A compact wideband dual-polarized base station antenna using asymmetric dipole," *IEEE Open J. Antennas Propag.*, vol. 3, pp. 189–195, 2022.

[16] K.-L. Wu, C. Wei, X. Mei, and Z.-Y. Zhang, "Array-antenna decoupling surface," *IEEE Trans. Antennas Propag.*, vol. 65, no. 12, pp. 6728–6738, Dec. 2017.

[17] C. Wei, Z.-Y. Zhang, and K.-L. Wu, "Phase compensation for decoupling of large-scale staggered dual-polarized dipole array antennas," *IEEE Trans. Antennas Propag.*, vol. 68, no. 4, pp. 2822–2831, Apr. 2020.

[18] D. He, Y. Chen, and S. Yang, "A low-profile triple-band shared-aperture antenna array for 5G base station applications," *IEEE Trans. Antennas Propag.*, vol. 70, no. 4, pp. 2732–2739, Apr. 2022.

[19] Y. Chen, J. Zhao, and S. Yang, "A novel stacked antenna configuration and its applications in dual-band shared-aperture base station antenna array designs," *IEEE Trans. Antennas Propag.*, vol. 67, no. 12, pp. 7234–7241, Dec. 2019.

[20] Y. Zhu, Y. Chen, and S. Yang, "Decoupling and low-profile design of dual-band dual-polarized base station antennas using frequency-selective surface," *IEEE Trans. Antennas Propag.*, vol. 67, no. 8, pp. 5272–5281, Aug. 2019.

[21] Y. F. Cao, X. Y. Zhang, and Q. Xue, "Compact shared-aperture dual-band dual-polarized array using filtering slot antenna and dual-function meta-surface," *IEEE Trans. Antennas Propag.*, vol. 70, no. 2, pp. 1120–1131, Feb. 2022.

[22] Y. Zhu, Y. Chen, and S. Yang, "Cross-band mutual coupling reduction in dual-band base-station antennas with a novel grid frequency selective surface," *IEEE Trans. Antennas Propag.*, vol. 69, no. 12, pp. 8991–8996, Dec. 2021.

[23] Y. Li and Q. Chu, "Coplanar dual-band base station antenna array using concept of cavity-backed antennas," *IEEE Trans. Antennas Propag.*, vol. 69, no. 11, pp. 7343–7354, Nov. 2021.

[24] W. Niu, B. Sun, G. Zhou, and Z. Lan, "Dual-band aperture shared antenna array with decreased radiation pattern distortion," *IEEE Trans. Antennas Propag.*, vol. 70, no. 7, pp. 6048–6053, Jul. 2022, doi: 10.1109/TAP.2022.3161267.

[25] Y. He, W. Huang, Z. He, L. Zhang, X. Gao, and Z. Zeng, "A novel cross-band decoupled shared-aperture base station antenna array unit for 5G mobile communications," *IEEE Open J. Antennas Propag.*, vol. 3, pp. 583–593, 2022.

[26] H.-H. Sun, C. Ding, H. Zhu, B. Jones, and Y. J. Guo, "Suppression of cross-band scattering in multiband antenna arrays," *IEEE Trans. Antennas Propag.*, vol. 67, no. 4, pp. 2379–2389, Apr. 2019.

[27] S. J. Yang, R. Ma, and X. Y. Zhang, "Self-decoupled dual-band dual-polarized aperture-shared antenna array," *IEEE Trans. Antennas Propag.*, vol. 70, no. 6, pp. 4890–4895, Jun. 2022.

[28] S. J. Yang, Y. Yang, and X. Y. Zhang, "Low scattering element-based aperture-shared array for multiband base stations," *IEEE Trans. Antennas Propag.*, vol. 69, no. 12, pp. 8315–8324, Dec. 2021.

[29] H.-H. Sun, H. Zhu, C. Ding, B. Jones, and Y. J. Guo, "Scattering suppression in a 4G and 5G base station antenna array using spiral chokes," *IEEE Antennas Wireless Propag. Lett.*, vol. 19, no. 10, pp. 1818–1822, Oct. 2020.

[30] D. He, Q. Yu, Y. Chen, and S. Yang, "Dual-band shared-aperture base station antenna array with electromagnetic transparent antenna elements," *IEEE Trans. Antennas Propag.*, vol. 69, no. 9, pp. 5596–5606, Sep. 2021.

[31] S. J. Yang and X. Y. Zhang, "Frequency selective surface-based dual-band dual-polarized high-gain antenna," *IEEE Trans. Antennas Propag.*, vol. 70, no. 3, pp. 1663–1671, Mar. 2022.

[32] X. Lu, Y. Chen, S. Guo, and S. Yang, "An electromagnetic-transparent cascade comb dipole antenna for multi-band shared-aperture base station antenna array," *IEEE Trans. Antennas Propag.*, vol. 70, no. 4, pp. 2750–2759, Apr. 2022.

[33] Y. Qin, R. Li, Q. Xue, X. Zhang, and Y. Cui, "Aperture-shared dual-band antennas with partially reflecting surfaces for base-station applications," *IEEE Trans. Antennas Propag.*, vol. 70, no. 5, pp. 3195–3207, May 2022.

[34] R. Lampe, "Design formulas for an asymmetric coplanar strip folded dipole," *IEEE Trans. Antennas Propag.*, vol. AP-33, no. 9, pp. 1028–1031, Sep. 1985.

[35] C. A. Balanis, *Antenna Theory Analysis and Design*, 3rd ed. New York, NY, USA: Wiley, 2005.

[36] T. Endo, Y. Sunahara, S. Satoh, and T. Katagi, "Resonant frequency and radiation efficiency of meander line antennas," *Electron. Commun. Jpn. II, Electron.*, vol. 83, no. 1, pp. 52–58, Jan. 2000.

[37] W. Hu et al., "Compact wideband folded dipole antenna with multi-resonant modes," *IEEE Trans. Antennas Propag.*, vol. 67, no. 11, pp. 6789–6799, Nov. 2019.

[38] F.-C. Chen, R.-S. Li, J.-M. Qiu, and Q.-X. Chu, "Sharp-rejection wideband bandstop filter using stepped impedance resonators," *IEEE Trans. Compon., Packag., Manuf. Technol.*, vol. 7, no. 3, pp. 444–449, Mar. 2017.

[39] C. F. Ding, X. Y. Zhang, Y. Zhang, Y. M. Pan, and Q. Xue, "Compact broadband dual-polarized filtering dipole antenna with high selectivity for base-station applications," *IEEE Trans. Antennas Propag.*, vol. 66, no. 11, pp. 5747–5756, Nov. 2018.

[40] B. A. Munk, *Frequency Selective Surfaces*. New York, NY, USA: Wiley, 2000.

Xuekang Liu (Graduate Student Member, IEEE) received the M.S. degree (Hons.) in the electromagnetic field and microwave technology from Xidian University, Xi'an, China, in 2020. He is currently pursuing the Ph.D. degree with the School of Engineering, University of Kent, Canterbury, U.K.

His current research interests include multiband base station antennas, filtering antennas, microstrip antennas, circularly polarized antennas, terminal antennas, and omnidirectional antennas.

Mr. Liu was a recipient of the Best Student Paper Award (Second Prize) from the 17th International Workshop on Antenna Technology (iWAT 2022), Dublin, and the Outstanding Academic Achievement for his M.S. program. He received the Young Scientist Award from the International Union of Radio Science (URSI) Member Committee, Germany, 2022.

Steven Gao (Fellow, IEEE) received the Ph.D. degree from Shanghai University, Shanghai, China, in 1999.

He is currently a Professor with the Department of Electronic Engineering, The Chinese University of Hong Kong, Hong Kong. Prior to this, he was a Chair Professor with the University of Kent, Kent, U.K., for nearly ten years. He has co-authored/co-edited three books, such as *Space Antenna Handbook* (Wiley, 2012), *Circularly Polarized Antennas* (IEEE & Wiley, 2014), and *Low-Cost Smart Antennas* (Wiley, 2019); over 400 articles; and 20 patents. His research covers smart antennas, phased arrays, MIMO, reconfigurable antennas, broadband/multiband antennas, satellite antennas, RF/microwave/mm-wave/THz circuits, mobile communications, satellite communications, UWB radars, synthetic aperture radars (SARs), sensors, the Internet of Things (IoT), and small satellites.

Dr. Gao is a fellow of the Royal Aeronautical Society and Institution of Engineering and Technology (IET). He served as the General Chair for international conferences, such as Loughborough Antennas and Propagation Conference (LAPC) in 2013 and UK, Europe, China Millimeter Waves and THz Technology Workshop (UCMMT) in 2021, and was an invited/keynote speaker at many conferences. He also serves as an Associate Editor for several international journals, such as IEEE TRANSACTIONS ON ANTENNAS AND PROPAGATION, *Radio Science*, *Electronics Letters*, and *IET Circuits, Devices and Systems*; and the Editor-in-Chief for Book Series on *Microwave and Wireless Technologies* (John Wiley & Sons). He is the Lead Guest Editor of IEEE TRANSACTIONS ON ANTENNAS AND PROPAGATION for a Special Issue on Low-Cost Wide-Angle Beam-Scanning Antennas in 2022. He served as the Lead Guest Editor for PROCEEDINGS OF THE IEEE for a Special Issue on Small Satellites in 2018 and IEEE TRANSACTIONS ON ANTENNAS AND PROPAGATION for a Special Issue on Antennas for Satellite Communication in 2015, and a Guest Editor for *IET Circuits, Devices, and Systems* for a Special Issue on Photonic and RF Communications Systems in 2014. He is the U.K.'s Representative at the European Association on Antennas and Propagation (EurAAP). He was a Distinguished Lecturer of the IEEE Antennas and Propagation Society.

Benito Sanz-Izquierdo (Member, IEEE) received the B.Sc. degree from the Universidad de Las Palmas de Gran Canaria (ULPGC), Las Palmas de Gran Canaria, Spain, and the M.Sc. and Ph.D. degrees from the University of Kent, Canterbury, U.K., in 2007.

In 2012, he worked with Harada Industries Ltd., Birmingham, U.K., where he developed novel antennas for the automotive industry. He was a Research Associate with the School of Engineering, University of Kent, in 2013, where he became a Lecturer in electronic systems and a Senior Lecturer in 2018. His research has been funded by a variety of sources, such as the U.K. Engineering and Physical Sciences Research Council (EPSRC), the Royal Academy of Engineering, and the Royal Society. His research interests include multiband antennas, wearable electronics, additive manufacturing (3-D printing), substrate integrated waveguides components, metamaterials, electromagnetic band-gap structures, frequency selective surfaces, and reconfigurable devices.

Dr. Sanz-Izquierdo has received awards and recognitions for his work on wearable antennas (mention in the House of Lords and the IEEE International Workshop on Antenna Technology (IWAT) Best Paper Award), frequency selective surfaces (the Best Paper at the Institution of Engineering and Technology (IET) Workshop on Aerospace Applications Award), and reconfigurable antennas (the 2017 CST University Publication Award for an IEEE TRANSACTIONS article), among others.

Haiwei Zhang received the B.S. and M.S. degrees in electronics engineering from Xidian University, Xi'an, China, in 2009 and 2012, respectively, and the Ph.D. degree in electronics engineering from the City University of Hong Kong, Hong Kong, in 2016.

He joined Huawei Technologies Company, Ltd., Chengdu, China, in 2016, where he was involved with the development of various antennas and RF components/sub-systems for the 5G and beyond wireless communications.

Dr. Zhang was awarded the Hong Kong Ph.D. Fellowship in 2012.

Lehu Wen (Member, IEEE) received the Ph.D. degree in electronic engineering from the University of Kent, Canterbury, U.K., in 2020.

He is currently a Research Associate with the School of Engineering, University of Kent. His research interests include wideband dual-polarized antennas, circularly polarized antennas, tightly coupled array antennas, and mobile terminal antennas.

Wei Hu (Member, IEEE) received the Ph.D. degree in electromagnetic fields and microwave technology from Xidian University, Xi'an, China, in 2013.

From 2013 to 2017, he was a Lecturer with the National Key Laboratory of Antennas and Microwave Technology, Collaborative Innovation Center of Information Sensing and Understanding, Xidian University, where he is currently an Associate Professor. From 2018 to 2019, he visited the University of Kent, Canterbury, Kent, U.K., as an Academic Visitor. He has authored or co-authored over 80 internationally refereed journal articles and has been serving as a reviewer for a number of technical journals and international conferences. His current research interests include multiband and wideband antennas, circularly polarized antennas, MIMO antenna arrays, and wideband wide-scanning phased arrays.

Qi Luo (Senior Member, IEEE) received the M.Sc. degree (Hons.) from The University of Sheffield, Sheffield, U.K., in 2006, and the Ph.D. degree (Hons.) from the University of Porto, Porto, Portugal, in 2012.

From 2012 to 2013, he worked with the University of Surrey, Guildford, U.K., as a Research Fellow. After that, he worked with the School of Engineering and Digital Arts, University of Kent, Canterbury, U.K., as a Senior Research Fellow. He is currently a Senior Lecturer with the School of Physics, Engineering, and Computer Science, University of Hertfordshire, Hatfield, U.K. His research interests include reflectarrays, transmitarrays, smart antennas, circularly polarized antennas, phased arrays, metasurfaces, multiband microstrip antennas, and electrically small antenna design.

Josaphat Tetuko Sri Sumantyo (Senior Member, IEEE) was born in Bandung, Indonesia, in 1970. He received the B.Eng. and M.Eng. degrees in electrical and computer engineering (subsurface radar systems) from Kanazawa University, Kanazawa, Japan, in 1995 and 1997, respectively, and the Ph.D. degree in artificial system sciences (applied radio wave and radar systems) from Chiba University, Chiba, Japan, in 2002.

From 2002 to 2005, he was a Lecturer (Post-Doctoral Fellowship Researcher) with the Center for Frontier Electronics and Photonics, Venture Business Laboratory, Chiba University. From 2005 to 2013, he was an Associate Professor (permanent staff) with the Center for Environmental Remote Sensing, Chiba University, where he is currently a Full Professor (permanent staff). He was the Head of the Department of Environmental Remote Sensing and the Head of the Division of Earth and Environmental Sciences, Graduate School of Integrated Science and Technology, Chiba University, from 2019 to 2020 and from 2022 to 2023. He has been the Head of the Disaster Information Analysis Research Division, Disaster Medical Research Center, Chiba University, since 2021. He has also been a Lecturer with the Department of Electrical Engineering, Faculty of Engineering, Universitas Sebelas Maret (UNS), Surakarta, Indonesia, since 2020. He has published about 930 journal and conference papers, and 15 book-related wave analyses, unmanned aerial vehicle (UAV), synthetic aperture radar (SAR), space antennas, and small antennas. His research interests include theoretically scattering microwave analysis and its applications in the microwave (radar) remote sensing, especially SAR, quantum radar, noise radar, and subsurface radar [very low frequency (VLF)], including InSAR, DInSAR, and PS-InSAR; analysis and design of antennas for mobile satellite communications and microwave sensors; and development of microwave sensors, including SAR for UAV, aircraft, high-altitude platform system (HAPS), and microsatellite.

Dr. Sri Sumantyo is also the General Chair of the Seventh and Eighth Asia-Pacific Conference on SAR (APSAR) in 2021 and 2023, and more than 290 invited talks and lectures. He is also the Co-Leader of the Technical Committee of Working Group on Remote Sensing Instrumentation and Technologies for UAV of IEEE-Geoscience and Remote Sensing Society (GRSS), the Technical Committee on Instrumentation, and the Future Technologies (IFT-TC), and has been an Associate Editor of IEEE GEOSCIENCE AND REMOTE SENSING LETTERS (GRSL) since 2021.

Xue-Xia Yang (Senior Member, IEEE) received the B.S. and M.S. degrees from Lanzhou University, Lanzhou, China, in 1991 and 1994, respectively, and the Ph.D. degree in the electromagnetic field and microwave technology from Shanghai University, Shanghai, China, in 2001.

From 1994 to 1998, she was a Teaching Assistant and a Lecturer with Lanzhou University. From 2001 to 2008, she was a Lecturer and an Associate Professor with Shanghai University, where she is currently a Professor and the Head of the Antennas and Microwave Research and Development Center. She has authored or co-authored over 180 technical journal and conference papers. Her research interests include antenna theory and technology, computational electromagnetics, and microwave power transmission.

Dr. Yang is a member of the Committee of the Antenna Society of the China Electronics Institute and a Senior Member of the China Electronics Institute. She is an Associate Editor of the *Journal of Shanghai University* (Science Edition). She is also a frequent reviewer of over ten scientific journals.